Modeling Dynamics and Function of Bone Marrow Cells in Mouse Liver Regeneration

Pedone, Elisa; Olteanu, Vlad-Aris; Marucci, Lucia; Isabel Munoz-Martin, Maria; Youssef, Sameh A.; de Bruin, Alain; Pia Cosma, Maria

Published in:
Cell reports

DOI:
10.1016/j.celrep.2016.12.008

Publication date:
2017

Article

Cell Reports

Modeling Dynamics and Function of Bone Marrow Cells in Mouse Liver Regeneration

Graphical Abstract

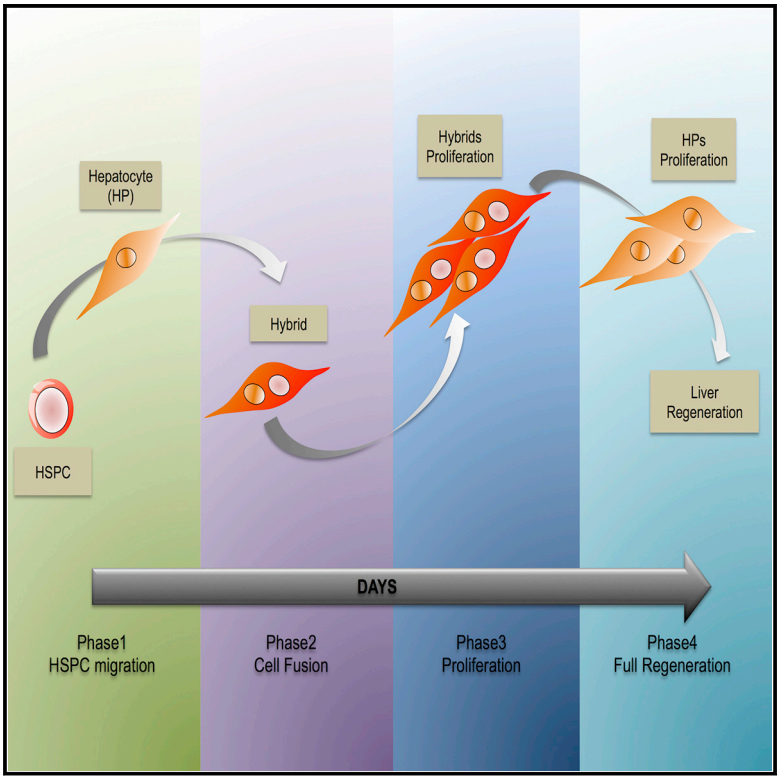

Authors

Elisa Pedone, Vlad-Aris Olteanu, Lucia Marucci, Maria Isabel Muñoz-Martin, Sameh A. Youssef, Alain de Bruin, Maria Pia Cosma

Correspondence

lucia.marucci@bristol.ac.uk (L.M.), pia.cosma@crg.es (M.P.C.)

In Brief

Hepatocyte replication is considered the main mechanism of liver regeneration after hepatectomy in mammals. Pedone et al. report that bone marrow cells can migrate into the liver upon resection and fuse with the hepatocytes. The derived hybrids are essential for efficient liver regeneration, which is also predicted by mathematical modeling.

Highlights

- Bone marrow cell migration after liver hepatectomy is key for liver regeneration
- Migrated bone marrow cells fuse with hepatocytes
- Hybrids are essential for liver regeneration
- Mathematical modeling unveils the hybrid function for liver regeneration

Pedone et al., 2017, Cell Reports *18*, 107–121
January 3, 2017
http://dx.doi.org/10.1016/j.celrep.2016.12.008

CellPress

Cell Reports
Article

Modeling Dynamics and Function of Bone Marrow Cells in Mouse Liver Regeneration

Elisa Pedone,[1,2] Vlad-Aris Olteanu,[3] Lucia Marucci,[1,3,*] Maria Isabel Muñoz-Martin,[1] Sameh A. Youssef,[4,5] Alain de Bruin,[4,6] and Maria Pia Cosma[1,2,7,8,*]

[1]Centre for Genomic Regulation (CRG), The Barcelona Institute of Science and Technology, Dr Aiguader 88, 08003 Barcelona, Spain
[2]Universitat Pompeu Fabra (UPF), Dr Aiguader 88, 08003 Barcelona, Spain
[3]Department of Engineering Mathematics, University of Bristol, Bristol BS8 1UB, UK
[4]Dutch Molecular Pathology Center, Department of Pathobiology, Faculty of Veterinary Medicine, Utrecht University, 3584 Utrecht, the Netherlands
[5]Department of Pathology, Alexandria Veterinary College, University of Alexandria-Egypt, 21612 Alexandria, Egypt
[6]University Medical Center Groningen, Department of Pediatrics, University of Groningen, 9713 Groningen, the Netherlands
[7]ICREA, Pg. Lluís Companys 23, 08010 Barcelona, Spain
[8]Lead Contact
*Correspondence: lucia.marucci@bristol.ac.uk (L.M.), pia.cosma@crg.es (M.P.C.)
http://dx.doi.org/10.1016/j.celrep.2016.12.008

SUMMARY

In rodents and humans, the liver can efficiently restore its mass after hepatectomy. This is largely attributed to the proliferation and cell cycle re-entry of hepatocytes. On the other hand, bone marrow cells (BMCs) migrate into the liver after resection. Here, we find that a block of BMC recruitment into the liver severely impairs its regeneration after the surgery. Mobilized hematopoietic stem and progenitor cells (HSPCs) in the resected liver can fuse with hepatocytes, and the hybrids proliferate earlier than the hepatocytes. Genetic ablation of the hybrids severely impairs hepatocyte proliferation and liver mass regeneration. Mathematical modeling reveals a key role of bone marrow (BM)-derived hybrids to drive proliferation in the regeneration process, and predicts regeneration efficiency in experimentally non-testable conditions. In conclusion, BM-derived hybrids are essential to trigger efficient liver regeneration after hepatectomy.

INTRODUCTION

Mathematical modeling is a powerful tool to describe complex biological processes, formalize interactions between components, analyze temporal dynamics, and predict the effects of perturbations (Kitano, 2002). Modeling has been used to describe liver functions and dynamics in mammals under normal and pathological conditions (Cook et al., 2015; Furchtgott et al., 2009; Holzhütter et al., 2012; Periwal et al., 2014).

The liver is the main detoxifying organ of the body, which can be injured by ingested toxins and infections. In response to these insults, hepatocytes can proliferate (Michalopoulos and DeFrances, 1997), and regeneration of the liver has evolved as a protective mechanism (Taub, 2004). Indeed, the mammalian liver displays a high regeneration potential (Fausto et al., 2006; Michalopoulos and DeFrances, 1997; Taub, 2004), and this phenomenon was described in rats a long time ago through the two-thirds partial hepatectomy model (Higgins and Anderson, 1931).

After partial hepatectomy, the remaining lobes grow and liver mass is restored in approximately 1 week in rodents (Duncan et al., 2009). The regeneration mechanism is largely attributed to the re-entry of the hepatocytes into the cell cycle and their proliferation (Fausto et al., 2006; Michalopoulos, 2007), which peaks 48 hr after resection in mice (Miyaoka et al., 2012). Cooperative signals induced by growth factors (such as hepatocyte, transforming, and epidermal growth factors, insulin, and glucagons) and cytokines (such as tumor necrosis factor and interleukin 6) are thought to be responsible for hepatocyte re-entry into the cell cycle, DNA replication, proliferation, and consequent liver mass regeneration (Costa et al., 2003).

However, there are still many unresolved key aspects in this process. The cell volume of hepatocytes enlarges (Gentric et al., 2012; Miyaoka et al., 2012), and there is a massive increase of hematopoietic stem cells (HSCs) in the peripheral blood and in the liver itself (De Silvestro et al., 2004; Fujii et al., 2002; Lemoli et al., 2006), whose role is not clear. In addition, there is some diverging evidence indicating that bone marrow (BM)-derived cells can either transdifferentiate in vivo in the mouse liver (Alison et al., 2000; Lagasse et al., 2000) or can fuse with hepatocytes in fumarylacetoacetate hydrolase (Fah)-deficient mice (Vassilopoulos et al., 2003; Wang et al., 2003).

Here, using modeling and experimental approaches, we prove a crucial role of bone marrow cells (BMCs) and of BM-hepatocyte hybrids in the dynamics and efficiency of mouse liver regeneration upon 30% and 70% partial hepatectomy. A mathematical model, fitted on experimental data, unveils the critical role of BMC recruitment and hybrid formation in enhancing proliferation and, ultimately, liver regeneration.

RESULTS

Mathematical Model Recapitulates the Dynamics of Mouse Liver Regeneration after Hepatectomy

In earlier work, a mathematical model for white rat liver regeneration upon partial hepatectomy was proposed (Furchtgott et al.,

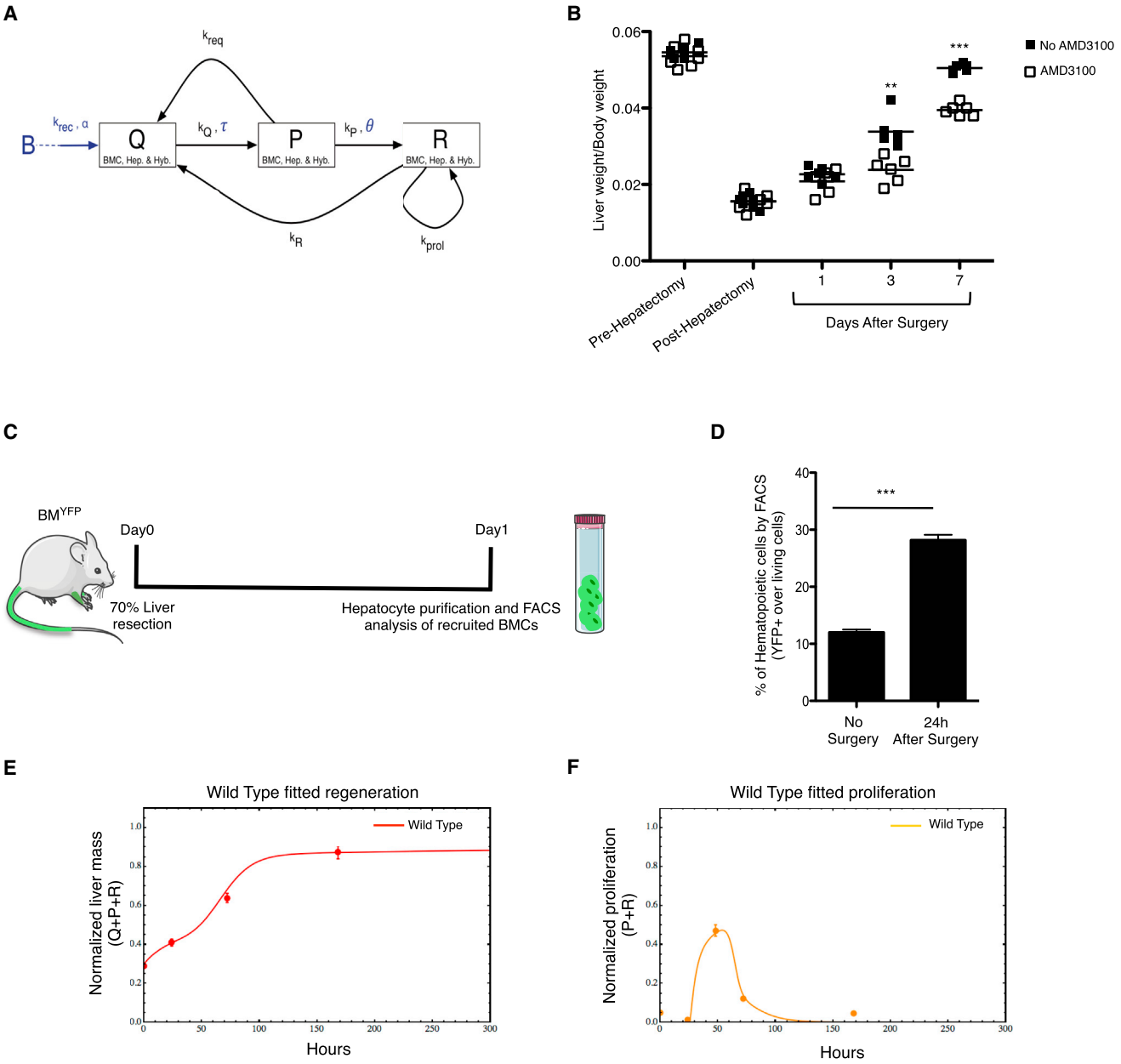

Figure 1. Derivation of a Mathematical Model Accounting for BMC Recruitment in the Liver upon 70% Partial Hepatectomy

(A) Schematic representation of cellular equations of the mathematical model. Blue font highlights the modifications to the rat model in Furchtgott et al. (2009). B, bone marrow cells; Q, P, and R, parameters as defined in the text and the Supplemental Experimental Procedures.

(B) Liver regeneration of wild-type mice treated or not treated with AMD3100, which was calculated as liver weight/body weight ratio at different days after PHx.

(C) Experimental scheme: recruitment of YFP+ cells into the liver of BM^{YFP} mice was analyzed by FACS 24 hr after PHx.

(D) Percentage of recruited YFP+ cells with respect to living cells (mixed parenchymal and bone marrow cell fractions) 24 hr after PHx. See Supplemental Experimental Procedures for details about cell purification.

(E and F) Simulations of the fitted model for liver mass regeneration (E) and proliferation (F) for wild-type mice ($BM^{CXCR4fl/fl}$) using normalized data from Figures 2C and S2D. Data are represented as mean ± SEM (n = 6, B and D). $p > 0.1$; $^{**}p < 0.01$; $^{***}p < 0.0001$.

See also Figure S1 and Table S1.

2009), which incorporates the main phenomenology and underlying signaling. Similarly, the mathematical formalism of our delay differential equations (DDEs) captures the rate of change in cell numbers, considering the three populations previously suggested to contribute to liver regeneration (Fausto et al., 2006): quiescent (Q), primed to replicate (P), and replicating (R) cells (Figure 1A). Coupled to cellular equations (Figure S1A), molecular equations describe immediate-early genes, cytokines,

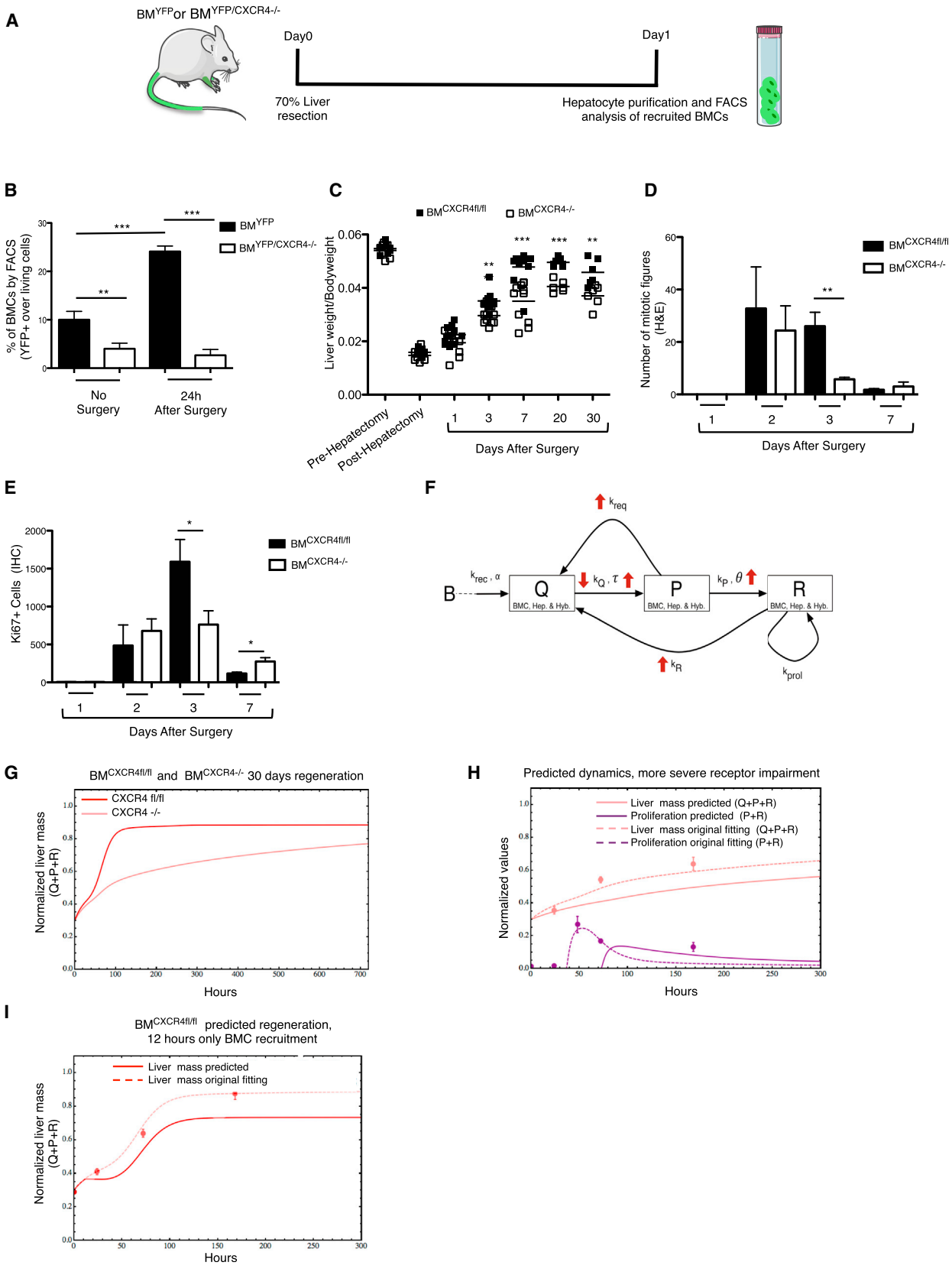

(legend on next page)

and growth factors that, activated upon liver resection, determine the transition among cell states (Figure S1B; Supplemental Experimental Procedures). The premise of our model is the focus on regeneration dynamics rather than on cellular species. Thus, we adapted the phenomenological parameters in the cellular equations, whereas the molecular equations and the related parameters were kept as intact as possible (Table S1). Notably, the same approach has been successfully used in adapting the rat model (Furchtgott et al., 2009) to reproduce data from humans (Periwal et al., 2014) because the biochemistry of liver regeneration is probably similar in different mammals.

To adapt the rat model, we noticed that, while in the rat, hepatocyte proliferation starts soon after hepatectomy (Furchtgott et al., 2009), in mice, the proliferation is delayed and peaks at 48 hr (Miyaoka et al., 2012; Weglarz and Sandgren, 2000). As expected, 24 hr upon 70% resection in wild-type mice, liver cells did not proliferate (Figure S1C) (Shu et al., 2009). We evaluated liver mass regeneration 7 days after resection (Figure 1B, no AMD3100) because this is a standard time range to analyze regeneration (Zhang et al., 2015). Interestingly, we observed a small but significant ($p < 0.0001$ between post-hepatectomy and day 1) increase in liver mass at day 1 (Figure 1B, day 1 no AMD3100) before cycling cells appeared (Figure S1C). This was likely due to the recruitment of hematopoietic cells in early stages of regeneration (De Silvestro et al., 2004; Lemoli et al., 2006). To confirm this hypothesis, we applied 70% liver resection to a group of transgenic mice expressing the yellow fluorescent protein (YFP) from the Rosa26-LoxP-stop-LoxP-YFP allele in the hematopoietic cells (BM^{YFP}) (Figure 1C). We found up to 30% of YFP+ cells in the liver, indicating a massive recruitment of hematopoietic cells within 24 hr from surgery (Figures 1D and S1D).

Next, to determine the identity of the recruited YFP+ cells, we examined the expression of markers of mature circulating blood cells or bone-marrow-derived progenitors. YFP+ cells expressed HSPC (c-kit+/sca1+) and granulocyte monocyte progenitor (GMP) (c-Kit+/Sca1−/Cd34+/Cd16.32+) markers (Figure S1E). In contrast, we excluded recruitment of cells from the peripheral blood because lineage-positive cells, such as B (B220+), T (Cd3+), and NK (CD49b+/CD3− and CD49b+/CD3+) cells, and macrophages (CD11b+ and CD11b+/F4-80+) did not increase into the resected liver after hepatectomy (Figure S1F), suggesting that recruited YFP+ cells include mostly BMCs.

Therefore, we changed the rat model to account for both the role that BMC mobilization can play in liver regeneration in a mouse and the different timing of hepatocyte proliferation and regeneration. We included an explicit term for BMC recruitment, and added two time delays (τ and θ) between the Q and P states and the P and R states (Figures 1A and S1A). We fitted the mathematical model to time-courses (7 day experiments) of wild-type mice that underwent hepatectomy; the dynamics of transition among the Q, P, and R states depend on BMC recruitment. The fitting accurately matches experimental proliferation and regeneration dynamics (Figures 1E and 1F).

BMC Mobilization Is Crucial for Hepatocyte Proliferation and Effective Regeneration

C-X-C motif chemokine receptor type 4 (CXCR4) and its ligand, SDF-1/CXCL12 (stromal cell-derived factor 1/C-X-C motif chemokine 12), are essential for the mobilization and migration of BMCs from the niche (Dalakas et al., 2005; Hatch et al., 2002; Kollet et al., 2003). Thus, to investigate if the recruitment of BMCs into the liver was critical for its regeneration, we analyzed BMC recruitment after 70% resection in the $CXCR4^{fl/fl}$/Vav-CRE/R26Y model, which carries BMCs deleted for CXCR4 and expressing YFP ($BM^{YFP/CXCR4-/-}$) (Figure 2A). Of note, $CXCR4^{fl/fl}$-Vav^{CRE} mice are normal and fertile and do not show apparent phenotypic defects, which could be ascribed to a bone marrow dysfunction. Indeed, it has been shown that Flt3-LSK cells in $CXCR4^{-/-}$ mice are in a normal number as compared to wild-type mice and sustained long-term hematopoiesis (Nie et al., 2008). Moreover, no major differences were found in the number of HSPCs in the fetal liver of $CXCR4^{-/-}$ E14.5 embryos as compared to wild-type mice (Foudi et al., 2006).

As opposed to the BM^{YFP} wild-type mice, we observed a massive impairment of YFP+ BMC recruitment in $BM^{YFP/CXCR4-/-}$ (Figures 2B and S2A). Importantly, liver regeneration in $BM^{CXCR4-/-}$ animals was severely compromised and, up to 30 days after resection, $BM^{CXCR4-/-}$ mice could not entirely restore their liver mass (Figure 2C). Moreover, the block of liver mass regeneration was associated with an impairment of liver cell proliferation; the mitotic index and Ki67+ cells measured in liver sections were drastically reduced 3 days after hepatectomy

Figure 2. CXCR4 Deletion in the BM Affects Cell Proliferation and Liver Regeneration after 70% PHx

(A) Experimental scheme: recruitment of YFP+ cells into the liver of BM^{YFP} and $BM^{YFP/CXCR4-/-}$ mice was analyzed by FACS 24 hr after PHx.

(B) Percentage of recruited YFP+ cells, which was calculated with respect to living cells (mixed parenchymal and bone marrow cell fractions) 24 hr after PHx in BM^{YFP} and $BM^{YFP/CXCR4-/-}$ mice.

(C) Liver regeneration of $BM^{CXCR4fl/fl}$ and $BM^{CXCR4-/-}$ mice, which was calculated as liver weight/body weight ratio at different days after PHx.

(D) Liver mitotic index of $BM^{CXCR4fl/fl}$ and $BM^{CXCR4-/-}$ mice following H&E staining at different days after PHx.

(E) Quantification of Ki67+ liver cells by immunohistochemistry (IHC) in $BM^{CXCR4fl/fl}$ and $BM^{CXCR4-/-}$ mice at different days after PHx.

(F) Scheme indicating, by red arrows, the variations of parameters fitting impaired mice data (i.e., $BM^{CXCR4-/-}$, toxin-treated, and AMD3100) versus values for respective control mice.

(G) 30-day simulated regeneration dynamics for $BM^{CXCR4fl/fl}$ and $BM^{CXCR4-/-}$ mice.

(H) Predicted $BM^{CXCR4-/-}$ regeneration and proliferation dynamics (solid lines) upon complete ablation of BMCs compared to the original fitting (dotted lines) and experimental data (dots, normalized data as in Figures S2F and S2G ± SEM).

(I) Prediction of regeneration dynamics (solid lines) when BMC recruitment is stopped after 12 hr in $BM^{CXCR4fl/fl}$ mice against original fitting (dotted lines) and experimental data (dots, normalized data as in Figures S2F and S2G ± SEM). Data are represented as mean ± SEM (n = 4, B and E; n = 5, D; n = 7, C). $p > 0.1$; *$p < 0.05$; **$p < 0.01$; ***$p < 0.0001$.

See also Figure S2 and Table S1.

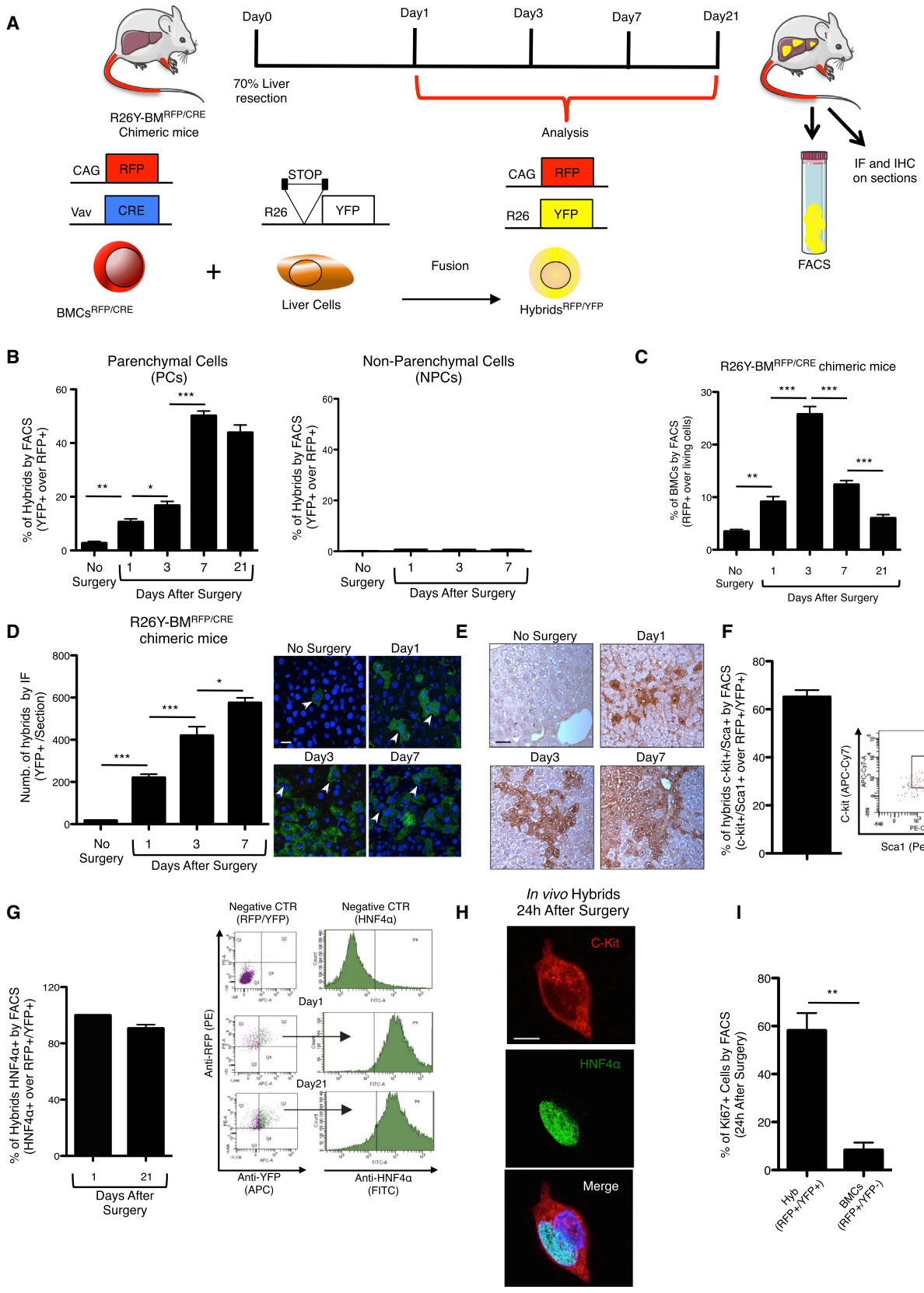

(legend on next page)

in BM$^{CXCR4-/-}$ mice (Figures 2D, 2E, S2B, and S2C). Reduction of proliferation was confirmed by fluorescence-activated cell sorting (FACS) analysis, although it was recovered at late time points after the surgery, likely representing a compensatory effect through late liver parenchymal cell replication (Figures S2D and S2E).

Model fitting confirmed the crucial role for BMCs in triggering the proliferation and, consequently, the regeneration processes. When reproducing regeneration and proliferation dynamics in BM$^{CXCR4-/-}$ mice (Figures S2F and S2G), k_Q (the parameter governing the propensity of cells to become primed to proliferate) was decreased, whereas k_{req} and k_R (the parameters describing the return to the quiescent state), as well as the two delays (τ and θ), were increased as compared to their values in the control conditions (Figure 2F; Table S1). Hence, by removing BMCs from the system, the transition of cells into a proliferative state is delayed and less effective, the transition from the primed to the replicating state is also delayed, and the sensitivity to requiescence signals is increased. Importantly, after simulating the model for a longer time (30 days), incomplete regeneration was observed in BM$^{CXCR4-/-}$ mice (Figure 2G).

Given that a small fraction of BMC population persists in BM$^{CXCR4-/-}$ mice (Figure 2B), the mathematical model was used to predict regeneration dynamics in the case of more severe reduction of BMCs. We found that the strength and timing of regeneration were further impaired compared to the actual experimental observations (Figure 2H).

Finally, we used the model to predict liver regeneration dynamics upon perturbation of BMC migration. Experimentally, it was not possible to assess for how long BMCs were recruited during the whole regeneration process. Thus, we ran simulations, stopping BMC recruitment 12 hr after resection. This resulted in a considerably impaired regeneration profile (Figure 2I), thereby suggesting that BMC recruitment should take place for at least 12 hr after surgery.

Upon Hepatectomy, Recruited BM Cells Fuse with Hepatocytes and the Hybrids Start to Proliferate Soon after Resection

Cell fusion is a well-known developmental process and an essential mechanism of regeneration after an injury (Johansson et al., 2008; Lluis and Cosma, 2010; Sanges et al., 2013, 2016; Sullivan and Eggan, 2006; Altarche-Xifro et al., 2016). We therefore aimed to investigate whether mobilized BMCs could fuse with liver cells and promote regeneration after hepatectomy. We subjected 70% liver resection to a group of chimeric mice carrying the R26Y transgene, in which the BM was replaced with a double transgenic CAG-RFP/VAV-CRE BM from donor mice (R26Y-BM$^{RFP/CRE}$) (Figure 3A). Vav-Cre is expressed only in the BM of transgenic mice (Stadtfeld and Graf, 2005); furthermore, we excluded its expression in liver cells. We found a limited number of positive cells in sections, which likely corresponded to liver resident hematopoietic cells (Figure S3A). Hepatectomy was performed 6 weeks after BM repopulation when peripheral blood and bone marrow chimerisms were around 30% and 42%, respectively (Figure S3B). Up to 3 days after resection, we found that 10%–15% of recruited RFP+ cells in the liver were also YFP+, indicating fusion events. This percentage increased to ~50% from 7 days up to 3 weeks after surgery, whereas recruited RFP+ cells decreased (Figures 3B, left plot, 3C, and S3C), suggesting an increase of hybrids and a decrease of BMCs in time in the resected liver. Importantly, we excluded major cell fusion events between BMCs and non-parenchymal liver cells (Figures 3B, right plot, and S3D). As the control experiment, to exclude a possible leakiness of the R26Y transgene and therefore expression of YFP independently of Cre-mediated STOP codon excision, we transplanted R26Y mice with a BM^{RFP} (not expressing Cre). After hepatectomy, we observed neither YFP+/RFP+ nor YFP+/RFP− cells in R26Y-BM^{RFP} chimeric mice (Figure S3C). Furthermore, we also excluded formation of hybrids in the BM and peripheral blood of R26Y-BM$^{RFP/CRE}$ (Figure S3B).

The increase of the hybrids at different days after surgery was also evident by counting the number of YFP+ cells for each section at different days after resection (Figure 3D). These results were also confirmed by immunohistochemistry on sections (Figure 3E). Of note, we found several YFP+ binucleated cells (arrows in Figure 3D).

The majority of the hybrids (YFP+/RFP+ population) were positive for markers of HSPCs (c-kit+/sca-1+) 1 day after hepatectomy (Figures 3F and S3E) and for the hepatocyte markers *Albumin*, hepatocyte nuclear factor 1 (*Hnf1*), and hepatocyte

Figure 3. BM-Recruited Cells Fuse with Parenchymal Cells after 70% PHx and the Hybrids Proliferate Soon After

(A) Experimental scheme: cell fusion was analyzed at different days after PHx in chimeric R26Y-BM$^{RFP/CRE}$ mice. Expression of the YFP occurs in the hybrids formed between BM$^{RFP/CRE}$ and liver cells^{R26Y} after excision of the floxed stop codon by CRE. Hybrids will also be RFP+.

(B) Percentage of YFP+ hybrids (PC-derived hybrids, left plot; NPC-derived hybrids, right plot), with respect to pre-gated RFP+ recruited BMCs at different days after PHx.

(C) Percentage of recruited RFP+ BMCs, which was calculated with respect to living cells (mixed parenchymal and bone marrow cell fractions) 1, 3, 7, and 21 days after surgery.

(D) Quantification of the YFP+ hybrids following immunofluorescence staining at different days after PHx in R26Y-BM$^{RFP/CRE}$ mice. Inset: representative images; arrows indicate binucleated cells.

(E) Representative IHC pictures of the YFP signal in sections of chimeric R26Y-BM$^{RFP/CRE}$ mice at different days after PHx.

(F) Percentage of c-kit+/sca-1+ cells, with respect to the total number of YFP+/RFP+ hybrids. Inset: representative FACS profile.

(G) Percentage of FACS-sorted hybrids (RFP+/YFP+) expressing the hepatocyte-specific marker HNF4α 1 day and 21 days after PHx. Inset: representative FACS profiles.

(H) HNF4α and c-Kit immunofluorescence on hybrids (RFP+/YFP+) sorted 24 hr after PHx in R26Y-BM$^{RFP/CRE}$.

(I) Percentage of Ki67+ hybrids (YFP+/RFP+) and BMCs (RFP+/YFP−) 24 hr after PHx in R26Y-BM$^{RFP/CRE}$ mice. Data are represented as mean ± SEM (n = 3, B [right plot], F, G, and I; n = 4, B [left plot] and C; n = 6, D). $p > 0.1$, $^*p < 0.05$; $^{**}p < 0.01$; $^{***}p < 0.0001$. Scale bar, 30 μm (D and E), 20 μm (H).

See also Figure S3.

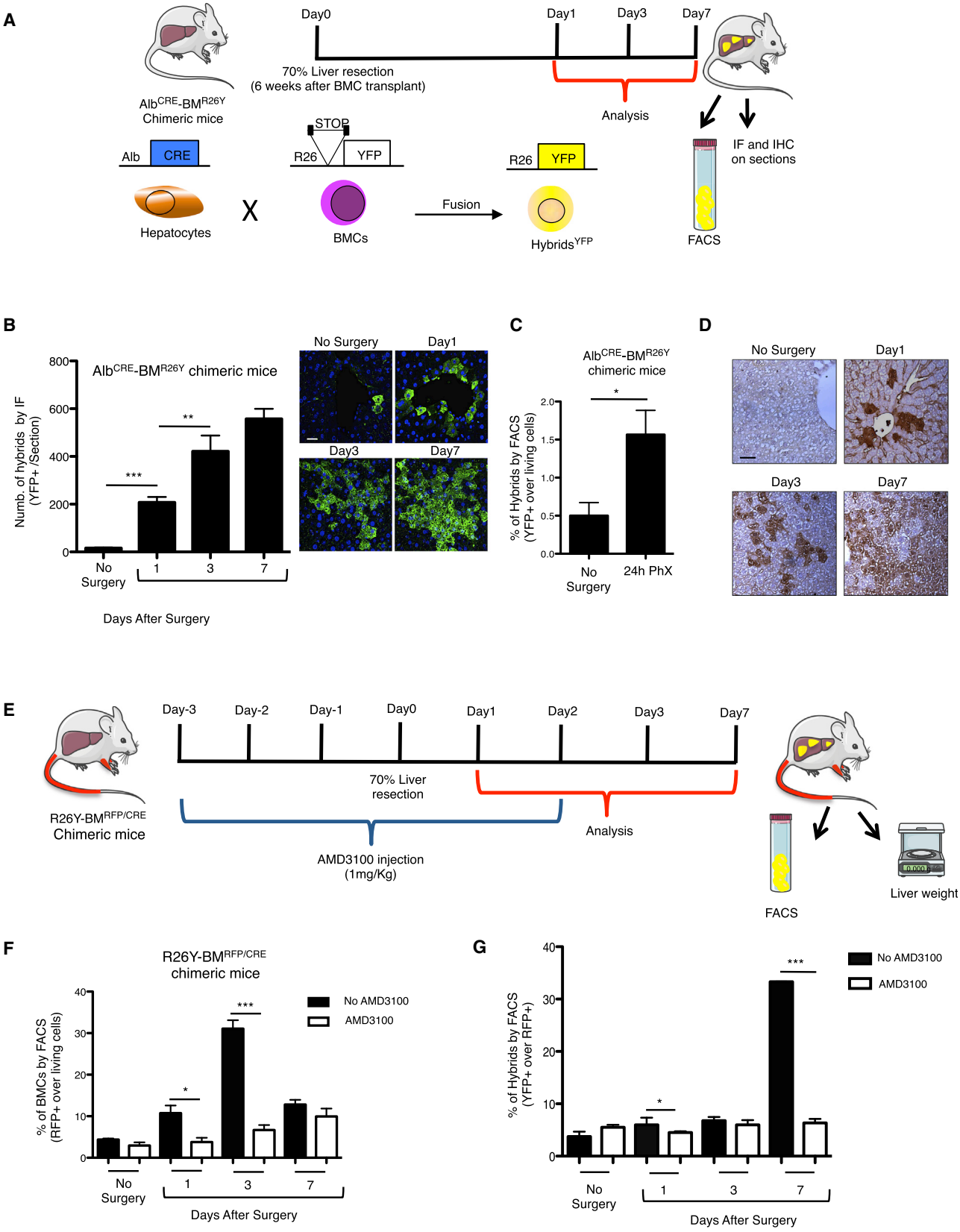

(legend on next page)

nuclear factor 4 alpha (HNF4α) from 1 day up to 21 days after surgery, indicating fusion of HSPCs with hepatocytes (Figures 3G and S3F). We confirmed these results by performing HNF4α and c-kit immunostaining on YFP+/RFP+ hybrids sorted from the livers of R26Y-BM$^{RFP/CRE}$ 24 hrs after surgery. We found cells that were positive for both HNF4α and c-Kit expression (Figure 3H). Furthermore, 24 hr after surgery, the hybrids expressed the cycling cell marker Ki67 and were polyploid (Figures 3I, S3G, and S3H). In contrast, the unfused BMCs (RFP+/YFP−) and parenchymal liver cells (PCs) did not express Ki67 at this time point (Figures 3I, S1C, and S3G).

In order to further prove whether the hepatocytes were BMC fusion partners, we used the hepatocyte-specific *Albumin*-CRE chimeric mice (Postic et al., 1999) carrying the R26Y bone marrow (Alb^{CRE}-BM^{R26Y}) (Figure 4A). The hybrids largely increased at different days after surgery (Figures 4B–4D), indicating fusion of BMCs with hepatocytes.

Finally, we observed that lineage-depleted bone marrow cells that are enriched for HSPCs could also fuse in vitro with PCs purified after liver hepatectomy, resulting in hybrids, which expressed HNF4α (Figures S4A and S4B). In contrast, lineage-positive cells did not fuse efficiently in vitro and neither did their fusion capability increase after hepatectomy (Figure S4A).

Overall, these results show that HSPCs can fuse with hepatocytes after liver resection and the hybrids have already entered the cell cycle 24 hr after the surgery, at a time when hepatocytes are still in the G0 resting phase of the cell cycle.

Because we showed that BMC migration in the liver of BM$^{CXCR4-/-}$ animals after hepatectomy is impaired, we then aimed to investigate whether this block of BMC recruitment affects hybrid formation. Thus, we injected the CXCR4 antagonist AMD3100 (De Clercq, 2009) into a group of chimeric R26Y-BM$^{RFP/CRE}$ mice, which received 70% liver resection and were analyzed from 24 hr to 7 days after the surgery (Figure 4E). In the group of AMD3100-treated mice, migration of RFP+ BMCs (Figure 4F) and fusion of the recruited BMCs with the hepatocytes (YFP+ over RFP+ cells) were largely reduced after the hepatectomy (Figures 4G and S4C). Interestingly, regeneration was largely impaired because liver mass corrected on body weight did not reach the level observed in the untreated mice (Figure 1B). Fitting the mathematical model on AMD3100-treated versus control mice, regeneration data confirmed impaired transition into the proliferative and replicating states, as in the comparison between BM$^{CXCR4-/-}$ and BM$^{CXCR4fl/fl}$ mice discussed above (Figure S4D; Table S1).

Of note, due to the lack of BMC recruitment in BM$^{YFP/CXCR4-/-}$ mice and the reduced fusion after CXCR4 inhibition by AMD3100, polyploidy was accordingly impaired in BM$^{CXCR4-/-}$ mice (Figure S4E), indicating the major contribution of BMC recruitment and bone-marrow-derived hybrids to liver regeneration after hepatectomy.

Liver Regeneration Is Impaired upon Selective Ablation of Hybrids and the Mathematical Model Correctly Predicts this Phenotype

To definitively prove that the hybrids play an essential role to induce liver regeneration, we used a mouse model that allows ablation of the hybrids in the liver after surgery. We obtained chimeric mice carrying the Rosa26-LoxP-STOP-LoxP-DTR (R26-diphtheria toxin receptor) transgene, in whom the BM was replaced with the CAG-RFP/VAV-CRE BM from donor mice (R26DTR-BM$^{RFP/CRE}$) (Buch et al., 2005). Upon 70% liver resection, BM-derived hybrids expressed both RFP and DTR, making them sensitive to diphtheria toxin injection; thus, they were selectively ablated (Figure 5A). We found a substantial, although not complete, ablation of the hybrids (DTR+ over RFP+ cells) in the liver at the different days after surgery, which, as expected, paralleled the reduction of RFP+ liver cells (Figures 4B and 4C). Leakiness of the R26DTR promoter was excluded because neither DTR+/RFP+ nor DTR+/RFP− cells were found in R26DTR-BM^{RFP} mice (not expressing Cre) (Figure S5A). Importantly, we noticed a significant impairment of liver regeneration in the group of toxin-treated mice (Figure 5D). Accordingly, we found a severe reduction of the cell mitotic index, Ki67+ cell number, and polyploidy in toxin-treated mice (Figures 5E, 5F, and S5B–S5F). As control, we excluded a possible toxic effect due to the toxin injection. This was tested in R26DTR mice and in R26DTR-BM^{RFP} mice, which both showed efficient liver regeneration after hepatectomy and toxin injection (Figure S5G). Furthermore, proliferation in R26DTR-BM^{RFP} mice after resection and toxin injection was in the normal expected range (Figure S5H).

Finally, we also generated chimeric Alb^{Cre}-BM^{R26DTR} and analyzed liver regeneration 7 days after surgery in vehicle and toxin-injected mice. Regeneration was severely impaired when hepatocyte-derived hybrids were selectively ablated (Figure 5G).

Figure 4. BMCs Fuse with Hepatocytes and a Block of BM Recruitment Significantly Affects Hybrid Formation

(A) Experimental scheme: cell fusion was analyzed by FACS, immunofluorescence (IF), and IHC after hepatectomy in chimeric Alb^{CRE}-BM^{R26Y} mice. Expression of the YFP occurs in the hybrids formed between BM^{R26Y} and hepatocytes$^{Alb/CRE}$ after excision of the floxed stop codon by CRE.

(B) Quantification of the YFP+ hybrids following immunofluorescence staining at different days after PHx in Alb^{CRE}-BM^{R26Y}mice. Inset: representative images.

(C) Percentage of YFP+ hybrids, which was calculated with respect to living cells (mixed parenchymal and bone marrow cell fractions) 24 hr after surgery.

(D) Representative IHC pictures of the YFP signal in sections of chimeric Alb^{CRE}-BM^{R26Y} mice at different days after PHx.

(E) Experimental scheme: cell fusion and liver mass regeneration was analyzed at different days after hepatectomy in chimeric R26Y-BM$^{RFP/CRE}$ mice upon CXCR4 inhibition by the antagonist AMD3100.

(F) Percentage of recruited RFP+ BMCs over living cells (mixed parenchymal and bone marrow cell fractions), which was measured 1, 3, and 7 days after surgery in the presence or without the presence of the CXCR4 antagonist AMD3100.

(G) Percentage of YFP+ hybrids, with respect to pre-gated RFP+ recruited BMCs at different days after PHx in the presence or without the presence of the CXCR4 antagonist AMD3100. Data are represented as mean ± SEM (n = 3, F and G; n = 4, C; n = 6, B). $p > 0.1$; *$p < 0.05$; **$p < 0.01$; ***$p < 0.0001$. Scale bar, 30 μm (B and D).

See also Figure S4.

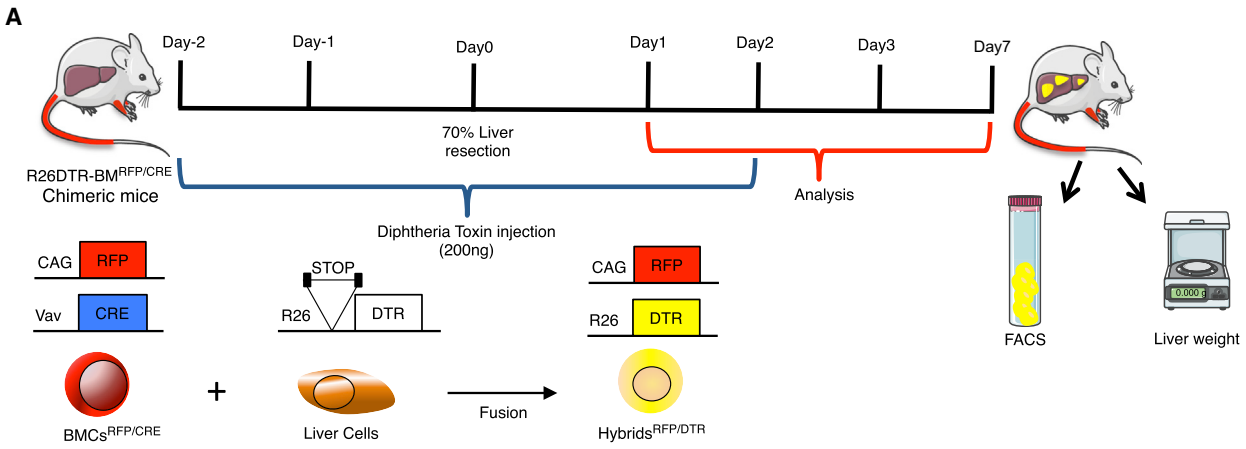

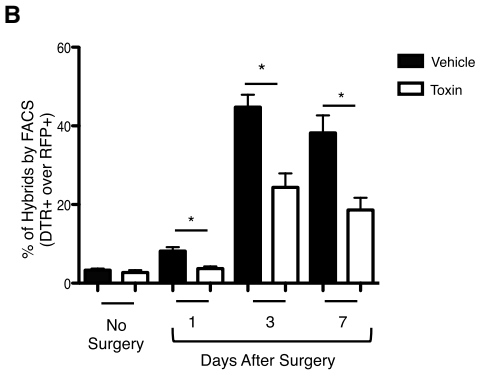

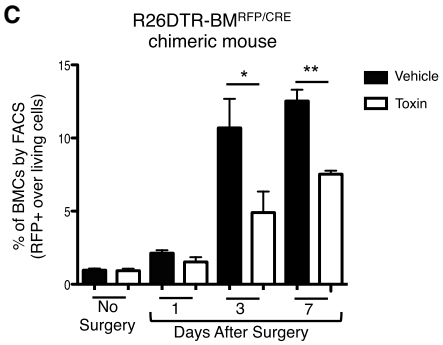

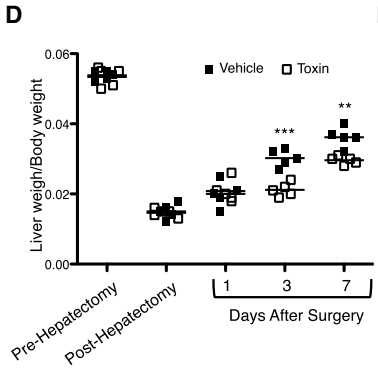

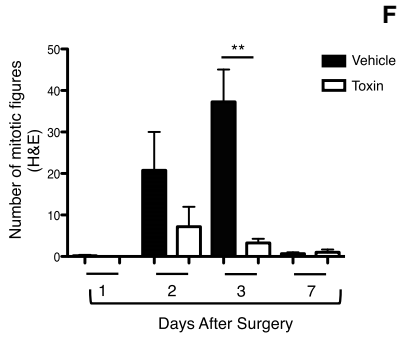

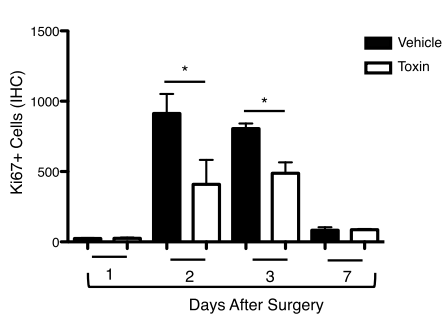

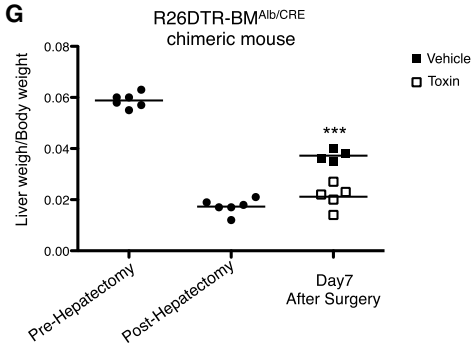

(legend on next page)

Next, we fitted liver regeneration dynamics upon selective hybrid elimination. The fitted model confirmed major cell proliferation defects (Figure 6A) and liver regeneration impairment (Figure 6B). Identified parameters (Table S1) indicate delayed and less efficient transitions of the cells both into the proliferative and replicating states (Figure 2F) as a consequence of the increased sensitivity to requiescence signals upon hybrid ablation. Moreover, no significant regeneration was observed in simulations of mice treated with toxin for up to 30 days (Figure 6C).

Of note, hybrids are included implicitly in the model rather than being modeled directly (Figures 1A and S1A). To confirm our fitting results, we additionally derived an extended model, which explicitly accounts for the contribution of hybrids formed by BMCs and hepatocytes (Figure S6A; see Supplemental Experimental Procedures for model derivation). Fitting the extended model on vehicle and toxin data (Figures 6D and 6E) confirmed the results obtained with the original model fitted on the same data-sets, i.e., alterations in the same parameters (Figure 2F; Table S2). Similar results were obtained with fitting the extended model on $BM^{CXCR4fl/fl}$ and $BM^{CXCR4-/-}$ data described above (Figures 6F and 6G; Table S2).

Recently, the existing formalism in Furchtgott et al. (2009) has been extended to include hypertrophy (Cook et al., 2015). Of note, the authors could reproduce experimental regeneration dynamics in a mouse (data from Shu et al., 2009), but failed in matching proliferation dynamics. This suggests that the addition of hypertrophy alone is insufficient to fully recapitulate mouse liver regeneration upon hepatectomy. We investigated whether taking hypertrophy into account would change our modeling results. An extended model that also accounts for hypertrophy, in addition to delays and BMC recruitment (Figure S6B; see Supplemental Experimental Procedures for model derivation), again confirmed the changes in parameters shown in Figure 2F when fitting $BM^{CXCR4fl/fl}$ $BM^{CXCR4-/-}$ data (Figures 6H and 6I; Table S3) while improving the quality of fitting presented previously (Cook et al., 2015).

In conclusion, it is possible to model hypertrophy or hybrids explicitly without affecting the main fitting results. Ablation of BMC-derived hybrids impairs proliferation of liver cells and, consequently, severely harms tissue regeneration after hepatectomy.

Mathematical Model Correctly Predicted Regeneration Dynamics and Proliferation upon 30% PHx

Finally, we carried out experiments in which liver resection was applied for 30% of the mass of $BM^{CXCR4fl/fl}$ and $BM^{CXCR4-/-}$ and of toxin-treated or untreated R26DTR-$BM^{RFP/CRE}$ mice. Data from the group of untreated R26DTR-$BM^{RFP/CRE}$ mice were used to fit 30% hepatectomy (Figure 7A), and the model correctly predicted the regeneration dynamics of $BM^{CXCR4fl/fl}$ mice upon 30% resection, matching experimental data (Figure 7B).

Interestingly, model simulations predicted the absence of proliferation and the synchronous dynamics of BMC recruitment and regeneration (Figure 7A). We validated these predictions. Indeed, also in agreement with previously published evidence (Mitchell et al., 2005), the proliferation of hepatocytes was not seen (Figures 7C and 7D). Liver regeneration normally occurred in $BM^{CXCR4fl/fl}$ and vehicle mice, whereas a full regeneration block was found in $BM^{CXCR4-/-}$ and toxin-sensitive mice (Figures 7E and 7F). The latter groups also displayed a severe hybrid loss (Figure 7G). The model, however, could not reproduce the 30% hepatectomy in impaired mice because the removal of hybrids and BMC recruitment, in both the original and the extended models, result in impairment of the parameter values relative to proliferation, which is absent in these experiments.

DISCUSSION

In this study, we have demonstrated the essential role of BMCs for liver regeneration in mice. We found that recruitment of HSPCs in the liver, their fusion with hepatocytes, and subsequent proliferation of the hybrids before that of the hepatocytes is essential for regeneration after hepatectomy.

Previous studies have indicated the importance of the proliferation of hepatocytes for liver regeneration (Duncan et al., 2009; Fausto et al., 2006; Michalopoulos, 2007). Alternatively, when hepatocyte replication is blocked, differentiation of ductal liver progenitor cells (oval cells) can play a crucial function (Itoh and Miyajima, 2014). Here, we introduced an additional layer of complexity to the picture, having identified the essential role of BM-derived hybrids in the regenerative process. Although we clearly showed that ablation of BM-derived hybrids significantly affects liver regeneration, it is still possible that ablation of an equivalent number of liver cells may affect the regeneration.

Figure 5. Selective Ablation of In Vivo Formed Hybrids Reduces Cell Proliferation and Impairs Liver Regeneration

(A) Experimental scheme: cell fusion and liver mass regeneration was analyzed at different days after PHx in chimeric R26DTR-$BM^{RFP/CRE}$ mice. Expression of the diphtheria toxin receptor (DTR) occurs in the hybrids formed between $BM^{RFP/CRE}$ and liver $cells^{R26DTR}$ after excision of the floxed stop codon by CRE. Hybrids will be RFP+/DTR+ and therefore sensitive to diphtheria toxin injection.

(B) Percentage of DTR+ hybrids, with respect to RFP+ recruited BMCs at different days after PHx.

(C) Percentage of recruited RFP+ BMCs over living cells (mixed parenchymal and bone marrow cell fractions), which was measured 1, 3, and 7 days after 70% PHx of R26DTR-$BM^{RFP/CRE}$ mice injected or not injected with diphtheria toxin.

(D) Liver regeneration of R26DTR-$BM^{RFP/CRE}$ mice treated or not treated with diphtheria toxin, which was calculated as liver weight/body weight at different days after PHx.

(E) Liver mitotic index of R26DTR-$BM^{RFP/CRE}$ mice treated or not treated with diphtheria toxin following H&E staining at different days after PHx.

(F) Quantification of Ki67+ liver cells by IHC in mice injected or not treated with diphtheria toxin at different days after PHx.

(G) Liver regeneration of R26DTR-$BM^{Alb/CRE}$ mice treated or not treated with diphtheria toxin, which was calculated as liver weight/body weight ratio 7 days after 70% PHx.

Circles indicate toxin- and vehicle- treated mice. Data are represented as mean ± SEM (n = 3, B and C; n = 4, E, F, and G; n = 5, D). $p > 0.1$; *$p < 0.05$; **$p < 0.01$; ***$p < 0.0001$.

See also Figure S5.

A

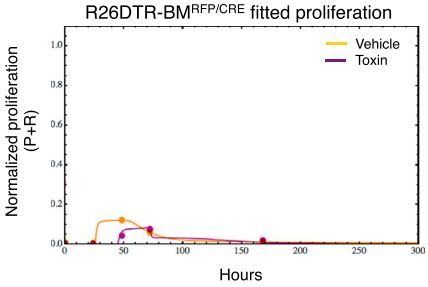

B

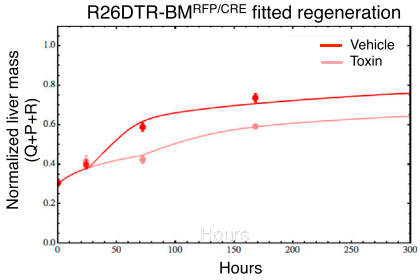

C

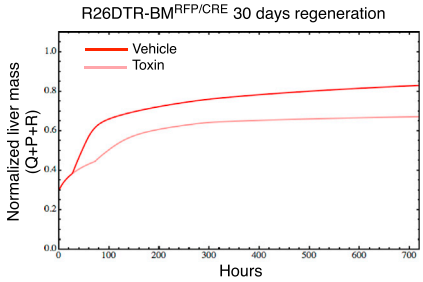

D

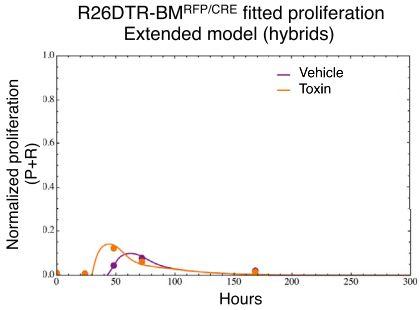

E

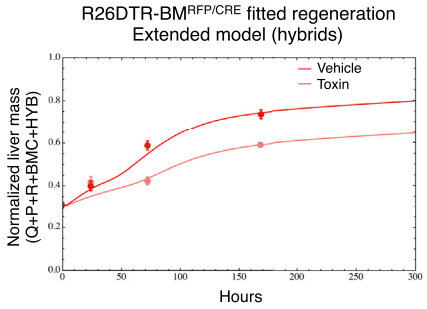

F

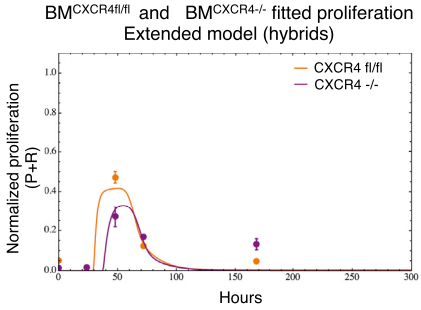

G

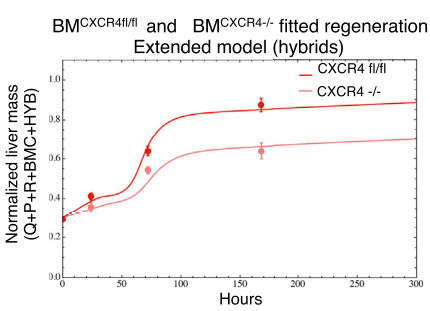

H

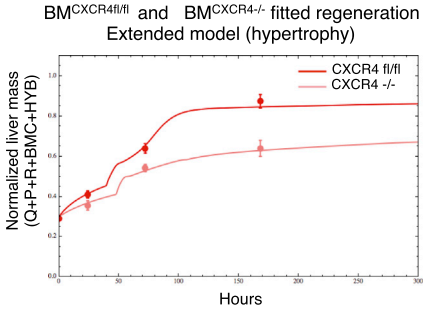

I

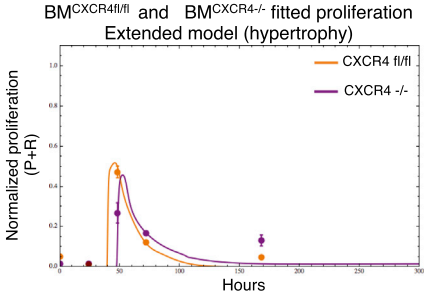

(legend on next page)

This could be tested in the future by generating mice carrying tunable DTR, which will allow ablation of hepatocytes in a mosaic fashion.

We showed that regeneration is blocked when CXCL12-CXCR4 is impaired in the BMCs, which thereby cannot migrate in the resected liver and fuse with the hepatocytes upon hepatectomy. On the other hand, we cannot exclude that a minimal fraction of resident hybrids formed before the hepatectomy could contribute to the regeneration of the liver. However, this appears to be independent of a possible function of the CXCL12-CXCR4 axis. The CXCL12-CXCR4 axis maintains hematopoietic stem cell quiescence (Nie et al., 2008), and it has been reported to increase proliferation of only hepatic oval cells (Hatch et al., 2002) or hepatic stem and cancer cells (Ghanem et al., 2014). Importantly, in our experimental system, the deletion of the CXCL12-CXCR4 axis was restricted to the BMCs, leaving the hepatic compartment and its possible proliferation unaffected.

Besides, with hepatocytes, BMCs can fuse with a variety of somatic cells in vivo, such as gut cells, muscle cells, and neurons (Lluis and Cosma, 2010). After BM-derived cell transplantation in damaged organs, the in-vivo-formed hybrids can regenerate the tissues, thereby providing a certain degree of functional recovery (Doyonnas et al., 2004; Johansson et al., 2008; Sanges et al., 2013, 2016; Altarche-Xifro et al., 2016). These observations indicate the importance of the hybrids in different regenerating tissue contexts.

The mammalian liver is highly polyploid. The ploidy increases with age, and it has been largely attributed to failed cytokinesis (Duncan and Soto-Gutierrez, 2013; Margall-Ducos et al., 2007). Polyploid hepatocytes are highly proliferative (Sigal et al., 1999; Weglarz et al., 2000) and can repopulate the host liver after transplantation in mice undergoing liver failure (Duncan et al., 2010). During regeneration, proliferating polyploid hepatocytes can also undergo multipolar mitosis and reduce their ploidy (Duncan et al., 2010). We observed binucleated and mononucleated cells, suggesting that heterokaryons might convert into synkaryons or reduce their ploidy during the regeneration process after the hepatectomy. Overall, liver function is fully maintained by polyploid cells and even by aneuploid hepatocytes (Duncan and Soto-Gutierrez, 2013).

In addition to failed cytokinesis, polyploid cells are formed by fusion with BMCs, as previously reported (Vassilopoulos et al., 2003; Wang et al., 2003) and our data here show. In the fumarylacetoacetate hydrolase knockout mice (Fah$^{-/-}$), hybrids formed upon fusion of BMCs with hepatocytes survived under selection pressure, i.e., upon withdrawal of the drug 2-(2-nitro-4-trifluoromethylbenzyol)-1,3-cyclohexanedione (NTBC), which prevents liver disease in Fah$^{-/-}$ mice (Vassilopoulos et al., 2003; Wang et al., 2003). Here, we observed formation of the hybrids without drug selection in a physiological model of liver regeneration, and discovered that they have a fundamental role for organ regeneration.

The function of this high ploidy was still not fully understood. Here, we demonstrated that proliferation of the hybrids before that of the hepatocytes is essential for liver mass regeneration after hepatectomy, clearly attributing a functional role to the polyploid cells. In addition, mathematical modeling showed that hybrid removal strongly impairs the regeneration process, delaying the transition of liver cells into a proliferative state and increasing the sensitivity to requiescence signals. Whether the newly formed hybrids directly trigger proliferation of the unfused hepatocytes, which enter in the cell cycle with a delay of 24 hr with respect to the hybrids, still needs to be defined.

We refined an existing mathematical model to account for the role of BMCs and hybrids in triggering regeneration, predicting regeneration efficiency in experimentally non-observable conditions. Our model explicitly considers BMCs while implicitly accounting for hybrids because BMCs are directly summed to the quiescent state (Supplemental Experimental Procedures). We opted for this approach because of limited experimental access to isolated hybrid dynamics in some of the mice used in this study (i.e., BM$^{CXCR4fl/fl}$ and BM$^{CXCR4-/-}$ animals). Nevertheless, extended formalisms, which include hybrids or that take into account hypertrophy as additional variables, confirmed results about the effect of impairment of BMC recruitment and hybrids on the system dynamics, confirming the power of our simplified approach.

Alternative mathematical formalisms describing liver physiology (reviewed in Holzhütter et al., 2012) account for multiscale levels of organization, extra-hepatic contribution (Diaz Ochoa et al., 2013), and the different nature of cells participating in pathology or regeneration (Hoehme et al., 2010). Our mathematical formalism has the potential to be extended to include spatial information and a more detailed description of the molecular processes involved in BM and hybrid-mediated regeneration; however, this would require the specification of additional parameters, which are at present not directly accessible experimentally. Although simple, our model has been parametrized by all available data and constitutes a first step in refining our quantitative understanding of regeneration and proliferation dynamics upon partial hepatectomy.

In humans, liver regeneration occurs after ischemia, toxic damage by alcohol, viral infection, or immune-mediated injury

Figure 6. Modeling the Contribution of BMC Recruitment and Cell Fusion to Cell Proliferation and Liver Regeneration Dynamics

(A and B) Simulations of the fitted model for proliferation (A) and liver mass (B) for R26DTR-BM$^{RFP/CRE}$ in toxin and vehicle-treated mice using normalized data from Figures 5D and S5D.

(C) 30-day simulated regeneration dynamics for R26DTR-BM$^{RFP/CRE}$ in toxin and vehicle-treated mice.

(D and E) Simulations of the fitted extended model (hybrids) for proliferation (D) and liver mass (E) for R26DTR-BM$^{RFP/CRE}$ toxin and vehicle-treated mice using normalized data from Figures 5D and S5D.

(F and G) Simulations of the fitted extended model (hybrids) for proliferation (F) and liver mass (G) for BM$^{CXCR4fl/fl}$ and BM$^{CXCR4-/-}$ mice using normalized data from Figures 2C and S2D.

(H and I) Simulations of the fitted extended model (hypertrophy) for liver mass (H) and proliferation (I) for BM$^{CXCR4fl/fl}$ and BM$^{CXCR4-/-}$ mice using normalized data from Figures 2C and S2D. See also Figure S6 and Tables S1, S2, and S3.

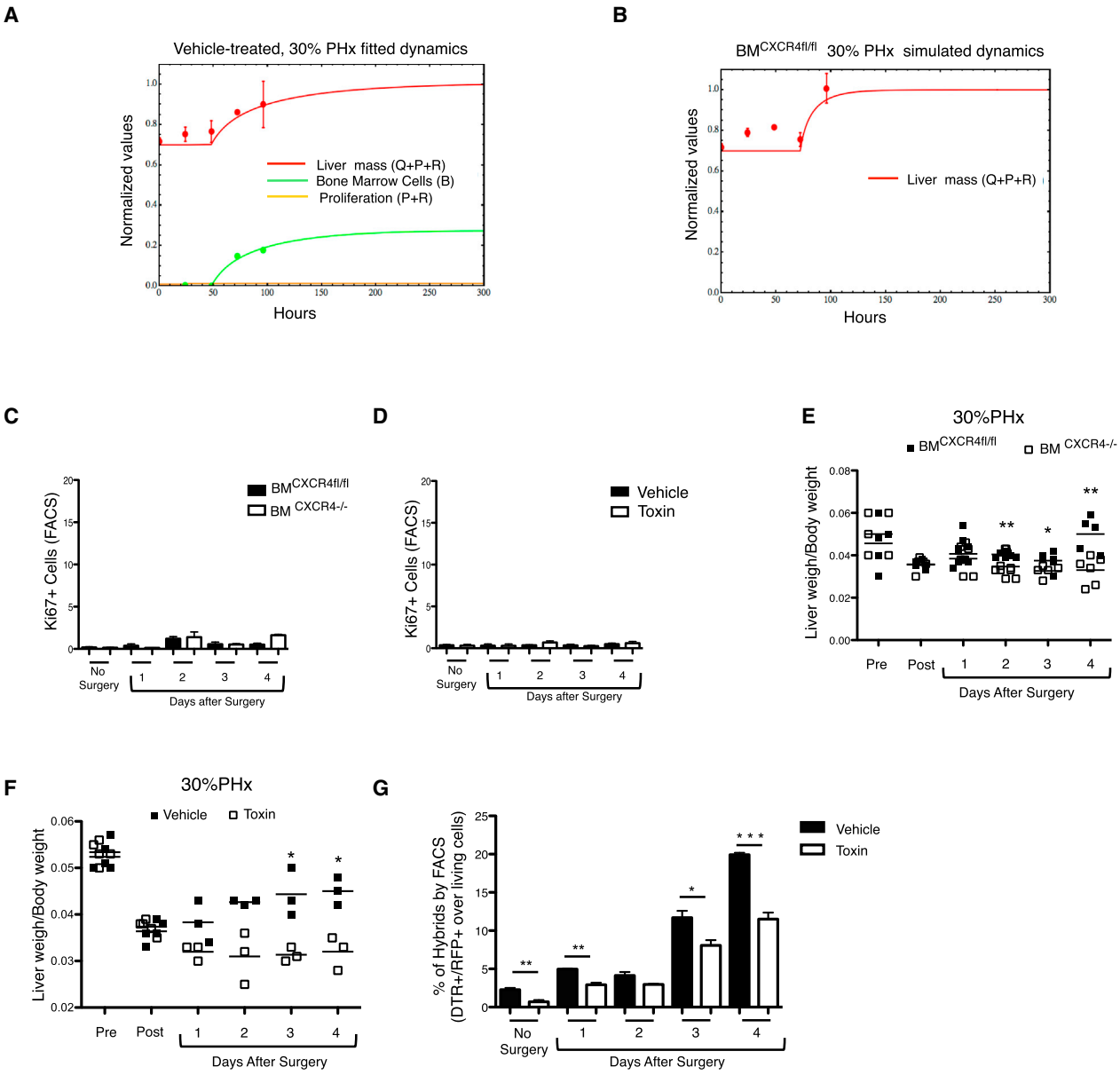

Figure 7. Modeling Simulations and Experimental Validations for the 30% PHx Model

(A) Fitted model simulations (solid lines) and experimental data (dots, normalized data from Figure 7F ± SEM) for regeneration, BMC recruitment, and proliferation dynamics upon 30% PHx in vehicle-treated mice.

(B) Prediction of regeneration dynamics (solid lines) for 30% PHx in $BM^{CXCR4fl/fl}$ mice against experimental data (dots, normalized data from Figure 7E ± SEM).

(C) Percentage of Ki67+ cells over parenchymal cells, which was measured by FACS 1, 2, 3, and 4 days after 30% PHx in $BM^{CXCR4fl/fl}$ and $BM^{CXCR4-/-}$.

(D) Percentage of Ki67+ cells over parenchymal cells, which was measured by FACS 1, 2, 3, and 4 days after 30% PHx in R26DTR-$BM^{RFP/CRE}$ chimeric mice treated or not treated with diphtheria toxin.

(E) Liver regeneration of $BM^{CXCR4fl/fl}$ and $BM^{CXCR4-/-}$ mice, which was calculated as liver weight/body weight ratio 1, 2, 3, and 4 days after 30% PHx.

(F) Liver regeneration of R26DTR-$BM^{RFP/CRE}$ chimeric mice treated or not treated with diphtheria toxin, which was calculated as liver weight/body weight ratio 1, 2, 3, and 4 days after 30% PHx.

(G) Percentage of in vivo formed hybrids between recruited $BM^{RFP/CRE}$ and parenchymal liver cells^{R26DTR} 1, 2, 3, and 4 days after 30% PHx in control mice and mice injected with diphtheria toxin. The percentage of hybrids (DTR+/RFP+) was calculated with respect to living cells (mixed parenchymal and bone marrow cell fractions). Data are represented as mean ± SEM (n = 3, C, D, F, and G; n = 5, E). $p > 0.1$, *$p < 0.05$; **$p < 0.01$; ***$p < 0.0001$.

See also Table S1.

(Koniaris et al., 2003). The liver regeneration mechanism should be fully dissected to elucidate how the liver responds to these types of insults and because partial resection is a current chirurgical practice for living liver donors. In contrast to rodents, the human liver regenerates more slowly, although efficiently for its function (Taub, 2004). Thus, the length of cell proliferation can diversify the mechanisms of liver regeneration in mammals. The early proliferation of BM-derived hybrids we found here can be potentially exploited, not only to improve regeneration after hepatectomy, but also for future attempts toward regenerative therapy in patients affected by liver failure.

EXPERIMENTAL PROCEDURES

Mice

All mice used in this study, R26Y [B6.129X1-Gt(ROSA)26Sor$^{tm1(EYFP)Cos}$/J] (Srinivas et al., 2001), BM$^{CXCR4fl/fl}$ [B6.129P2-Cxcr4^{tm2Yzo}/J] (Ephrussi and St Johnston, 2004), CAG-RFP [B6.Cg-Tg(CAG-mRFP1)1F1 Hadj/J] (Gregor et al., 2005), R26DTR [C57BL/6-Gt(ROSA) 26Sortm1(HBEGF)Awai/J] (Buch et al., 2005), Vav-Cre (Stadtfeld and Graf, 2005), and Alb-CRE [B6.Cg-Tg(Alb-Cre)21Mgn/J] (Postic et al., 1999), were kept in a barrier and SPF animal facility in accordance with the CEEA (Ethical Committee for Animal Experimentation) of the Government of Catalonia. Males and females between 9 and 12 weeks were used for the experiments.

Flow Cytometry and Cell Sorting

Mice were euthanized with CO_2 and perfused with PBS until the liver lobes drained off the blood and appeared pale. Liver samples were collected, and cells were purified by a double disaggregation step, as described in the Supplemental Experimental Procedures. Purified cells were pelleted and resuspended in PBS with 2% FCS with DAPI and analyzed using a BD LSR Fortessa (see Supplemental Experimental Procedures for more details). For cell sorting of in vitro and in vivo formed hybrids, samples were prepared as reported above and sorted using a BD FACS aria II.

Statistical Analysis

The percentage of recruited BMCs, hybrids (in vivo and in vitro formed), and cycling cells (Ki67+) was measured by FACS and calculated using the BD FACSDiva software. For quantification of YFP+ hybrids (three random fields for each mouse) and Ki67+ hepatocytes (five random fields for each mouse) in liver sections, we used image processing tools in ImageJ software (US NIH; http://rsb.info.nih.gov/ij). Data are reported as mean ± SEM, and the number of replicates is specified in the figure legends. Differences were examined using two-tailed unpaired Student's t tests, and $p < 0.05$ was considered significant.

SUPPLEMENTAL INFORMATION

Supplemental Information includes Supplemental Experimental Procedures, six figures, and three tables and can be found with this article online at http://dx.doi.org/10.1016/j.celrep.2016.12.008.

AUTHOR CONTRIBUTIONS

Conceptualization, M.P.C., E.P., and L.M.; Methodology, E.P. and M.I.M.-M.; Formal Analysis, L.M. and V.A.O.; Investigation, E.P., M.I.M.-M., and S.A.Y.; Writing – Original draft, M.P.C., E.P., L.M., and V.A.O.; Writing – Review & Editing, M.P.C., E.P., L.M., and V.A.O.; Visualization, M.P.C., E.P., L.M., and V.A.O.; Supervision, M.P.C., L.M., and A.d.B.; Project Administration, M.P.C.; Funding Acquisition, M.P.C. and L.M.

ACKNOWLEDGMENTS

We thank M. di Bernardo, M. Homer (Bristol University, UK), and J. Sharpe (CRG, Barcelona) for suggestions on the manuscript; UPF Flow Cytometry; CRG microscopy and histology core facilities; and the PRBB animal facility. This work was supported by an ERC grant (242630-RERE to M.P.C.), the Ministerio de Economia y Competitividad and FEDER funds (SAF2011-28580, BFU2014-54717-P, and BFU2015-71984-ERC to M.P.C.), an AGAUR grant from Secretaria d'Universitats i Investigació del Departament d'Economia i Coneixement de la Generalitat de Catalunya (2014SGR1137 to M.P.C.), an MRC grant (MR/N021444/1 to L.M.), BrisSynBio, BBSRC/EPSRC Synthetic Biology Research Centre (BB/L01386X/1 to L.M.), and Engineering and Physical Sciences Research Council (EP/I013717/1 to V.A.O.). We acknowledge support of the Spanish Ministry of Economy and Competitiveness, Centro de Excelencia Severo Ochoa 2013-2017 and of the CERCA Programme/Generalitat de Catalunya.

Received: April 14, 2016
Revised: July 15, 2016
Accepted: December 1, 2016
Published: January 3, 2017

REFERENCES

Alison, M.R., Poulsom, R., Jeffery, R., Dhillon, A.P., Quaglia, A., Jacob, J., Novelli, M., Prentice, G., Williamson, J., and Wright, N.A. (2000). Hepatocytes from non-hepatic adult stem cells. Nature *406*, 257.

Altarche-Xifro, W., di Vicino, U., Muñoz-Martin, M.I., Bortolozzi, A., Bové, J., Vila, M., and Cosma, M.P. (2016). Functional rescue of dopaminergic neuron loss in Parkinson's disease mice after transplantation of hematopoietic stem and progenitor cells. EBioMedicine *8*, 83–95.

Buch, T., Heppner, F.L., Tertilt, C., Heinen, T.J., Kremer, M., Wunderlich, F.T., Jung, S., and Waisman, A. (2005). A Cre-inducible diphtheria toxin receptor mediates cell lineage ablation after toxin administration. Nat. Methods *2*, 419–426.

Cook, D., Ogunnaike, B.A., and Vadigepalli, R. (2015). Systems analysis of non-parenchymal cell modulation of liver repair across multiple regeneration modes. BMC Syst. Biol. *9*, 71.

Costa, R.H., Kalinichenko, V.V., Holterman, A.X., and Wang, X. (2003). Transcription factors in liver development, differentiation, and regeneration. Hepatology *38*, 1331–1347.

Dalakas, E., Newsome, P.N., Harrison, D.J., and Plevris, J.N. (2005). Hematopoietic stem cell trafficking in liver injury. FASEB J. *19*, 1225–1231.

De Clercq, E. (2009). The AMD3100 story: the path to the discovery of a stem cell mobilizer (Mozobil). Biochem. Pharmacol. *77*, 1655–1664.

De Silvestro, G., Vicarioto, M., Donadel, C., Menegazzo, M., Marson, P., and Corsini, A. (2004). Mobilization of peripheral blood hematopoietic stem cells following liver resection surgery. Hepatogastroenterology *51*, 805–810.

Diaz Ochoa, J.G., Bucher, J., Péry, A.R., Zaldivar Comenges, J.M., Niklas, J., and Mauch, K. (2013). A multi-scale modeling framework for individualized, spatiotemporal prediction of drug effects and toxicological risk. Front. Pharmacol. *3*, 204.

Doyonnas, R., LaBarge, M.A., Sacco, A., Charlton, C., and Blau, H.M. (2004). Hematopoietic contribution to skeletal muscle regeneration by myelomonocytic precursors. Proc. Natl. Acad. Sci. USA *101*, 13507–13512.

Duncan, A.W., and Soto-Gutierrez, A. (2013). Liver repopulation and regeneration: new approaches to old questions. Curr. Opin. Organ Transplant. *18*, 197–202.

Duncan, A.W., Dorrell, C., and Grompe, M. (2009). Stem cells and liver regeneration. Gastroenterology *137*, 466–481.

Duncan, A.W., Taylor, M.H., Hickey, R.D., Hanlon Newell, A.E., Lenzi, M.L., Olson, S.B., Finegold, M.J., and Grompe, M. (2010). The ploidy conveyor of mature hepatocytes as a source of genetic variation. Nature *467*, 707–710.

Ephrussi, A., and St Johnston, D. (2004). Seeing is believing: the bicoid morphogen gradient matures. Cell *116*, 143–152.

Fausto, N., Campbell, J.S., and Riehle, K.J. (2006). Liver regeneration. Hepatology *43* (*Suppl 1*), S45–S53.

Foudi, A., Jarrier, P., Zhang, Y., Wittner, M., Geay, J.F., Lecluse, Y., Nagasawa, T., Vainchenker, W., and Louache, F. (2006). Reduced retention of radioprotective hematopoietic cells within the bone marrow microenvironment in CXCR4-/- chimeric mice. Blood *107*, 2243–2251.

Fujii, H., Hirose, T., Oe, S., Yasuchika, K., Azuma, H., Fujikawa, T., Nagao, M., and Yamaoka, Y. (2002). Contribution of bone marrow cells to liver regeneration after partial hepatectomy in mice. J. Hepatol. *36*, 653–659.

Furchtgott, L.A., Chow, C.C., and Periwal, V. (2009). A model of liver regeneration. Biophys. J. *96*, 3926–3935.

Gentric, G., Celton-Morizur, S., and Desdouets, C. (2012). Polyploidy and liver proliferation. Clin. Res. Hepatol. Gastroenterol. *36*, 29–34.

Ghanem, I., Riveiro, M.E., Paradis, V., Faivre, S., de Parga, P.M., and Raymond, E. (2014). Insights on the CXCL12-CXCR4 axis in hepatocellular carcinoma carcinogenesis. Am J Transl Res. *6*, 340–352.

Gregor, T., Bialek, W., de Ruyter van Steveninck, R.R., Tank, D.W., and Wieschaus, E.F. (2005). Diffusion and scaling during early embryonic pattern formation. Proc. Natl. Acad. Sci. USA *102*, 18403–18407.

Hatch, H.M., Zheng, D., Jorgensen, M.L., and Petersen, B.E. (2002). SDF-1alpha/CXCR4: a mechanism for hepatic oval cell activation and bone marrow stem cell recruitment to the injured liver of rats. Cloning Stem Cells *4*, 339–351.

Higgins, G.M., and Anderson, R.M. (1931). Experimental pathology of the liver. I. Restoration of the liver of the white rat following partial surgical removal. Arch. Pathol. (Chic) *12*, 186–202.

Hoehme, S., Brulport, M., Bauer, A., Bedawy, E., Schormann, W., Hermes, M., Puppe, V., Gebhardt, R., Zellmer, S., Schwarz, M., et al. (2010). Prediction and validation of cell alignment along microvessels as order principle to restore tissue architecture in liver regeneration. Proc. Natl. Acad. Sci. USA *107*, 10371–10376.

Holzhütter, H.G., Drasdo, D., Preusser, T., Lippert, J., and Henney, A.M. (2012). The virtual liver: a multidisciplinary, multilevel challenge for systems biology. Wiley Interdiscip. Rev. Syst. Biol. Med. *4*, 221–235.

Itoh, T., and Miyajima, A. (2014). Liver regeneration by stem/progenitor cells. Hepatology *59*, 1617–1626.

Johansson, C.B., Youssef, S., Koleckar, K., Holbrook, C., Doyonnas, R., Corbel, S.Y., Steinman, L., Rossi, F.M., and Blau, H.M. (2008). Extensive fusion of haematopoietic cells with Purkinje neurons in response to chronic inflammation. Nat. Cell Biol. *10*, 575–583.

Kitano, H. (2002). Computational systems biology. Nature *420*, 206–210.

Kollet, O., Shivtiel, S., Chen, Y.Q., Suriawinata, J., Thung, S.N., Dabeva, M.D., Kahn, J., Spiegel, A., Dar, A., Samira, S., et al. (2003). HGF, SDF-1, and MMP-9 are involved in stress-induced human CD34+ stem cell recruitment to the liver. J. Clin. Invest. *112*, 160–169.

Koniaris, L.G., McKillop, I.H., Schwartz, S.I., and Zimmers, T.A. (2003). Liver regeneration. J. Am. Coll. Surg. *197*, 634–659.

Lagasse, E., Connors, H., Al-Dhalimy, M., Reitsma, M., Dohse, M., Osborne, L., Wang, X., Finegold, M., Weissman, I.L., and Grompe, M. (2000). Purified hematopoietic stem cells can differentiate into hepatocytes in vivo. Nat. Med. *6*, 1229–1234.

Lemoli, R.M., Catani, L., Talarico, S., Loggi, E., Gramenzi, A., Baccarani, U., Fogli, M., Grazi, G.L., Aluigi, M., Marzocchi, G., et al. (2006). Mobilization of bone marrow-derived hematopoietic and endothelial stem cells after orthotopic liver transplantation and liver resection. Stem Cells *24*, 2817–2825.

Lluis, F., and Cosma, M.P. (2010). Cell-fusion-mediated somatic-cell reprogramming: a mechanism for tissue regeneration. J. Cell. Physiol. *223*, 6–13.

Margall-Ducos, G., Celton-Morizur, S., Couton, D., Brégerie, O., and Desdouets, C. (2007). Liver tetraploidization is controlled by a new process of incomplete cytokinesis. J. Cell Sci. *120*, 3633–3639.

Michalopoulos, G.K. (2007). Liver regeneration. J. Cell. Physiol. *213*, 286–300.

Michalopoulos, G.K., and DeFrances, M.C. (1997). Liver regeneration. Science *276*, 60–66.

Mitchell, C., Nivison, M., Jackson, L.F., Fox, R., Lee, D.C., Campbell, J.S., and Fausto, N. (2005). Heparin-binding epidermal growth factor-like growth factor links hepatocyte priming with cell cycle progression during liver regeneration. J. Biol. Chem. *280*, 2562–2568.

Miyaoka, Y., Ebato, K., Kato, H., Arakawa, S., Shimizu, S., and Miyajima, A. (2012). Hypertrophy and unconventional cell division of hepatocytes underlie liver regeneration. Curr. Biol. *22*, 1166–1175.

Nie, Y., Han, Y.C., and Zou, Y.R. (2008). CXCR4 is required for the quiescence of primitive hematopoietic cells. J. Exp. Med. *205*, 777–783.

Periwal, V., Gaillard, J.R., Needleman, L., and Doria, C. (2014). Mathematical model of liver regeneration in human live donors. J. Cell. Physiol. *229*, 599–606.

Postic, C., Shiota, M., Niswender, K.D., Jetton, T.L., Chen, Y., Moates, J.M., Shelton, K.D., Lindner, J., Cherrington, A.D., and Magnuson, M.A. (1999). Dual roles for glucokinase in glucose homeostasis as determined by liver and pancreatic beta cell-specific gene knock-outs using Cre recombinase. J. Biol. Chem. *274*, 305–315.

Sanges, D., Simonte, G., Di Vicino, U., Romo, N., Pinilla, I., Nicolás, M., and Cosma, M.P. (2016). Reprogramming Müller glia via in vivo cell fusion regenerates murine photoreceptors. J. Clin. Invest. *126*, 3104–3116.

Sanges, D., Romo, N., Simonte, G., Di Vicino, U., Tahoces, A.D., Fernández, E., and Cosma, M.P. (2013). Wnt/β-catenin signaling triggers neuron reprogramming and regeneration in the mouse retina. Cell Rep. *4*, 271–286.

Shu, R.Z., Zhang, F., Wang, F., Feng, D.C., Li, X.H., Ren, W.H., Wu, X.L., Yang, X., Liao, X.D., Huang, L., et al. (2009). Adiponectin deficiency impairs liver regeneration through attenuating STAT3 phosphorylation in mice. Lab. Invest. *89*, 1043–1052.

Sigal, S.H., Rajvanshi, P., Gorla, G.R., Sokhi, R.P., Saxena, R., Gebhard, D.R., Jr., Reid, L.M., and Gupta, S. (1999). Partial hepatectomy-induced polyploidy attenuates hepatocyte replication and activates cell aging events. Am. J. Physiol. *276*, G1260–G1272.

Srinivas, S., Watanabe, T., Lin, C.S., William, C.M., Tanabe, Y., Jessell, T.M., and Costantini, F. (2001). Cre reporter strains produced by targeted insertion of EYFP and ECFP into the ROSA26 locus. BMC Dev. Biol. *1*, 4.

Stadtfeld, M., and Graf, T. (2005). Assessing the role of hematopoietic plasticity for endothelial and hepatocyte development by non-invasive lineage tracing. Development *132*, 203–213.

Sullivan, S., and Eggan, K. (2006). The potential of cell fusion for human therapy. Stem Cell Rev. *2*, 341–349.

Taub, R. (2004). Liver regeneration: from myth to mechanism. Nat. Rev. Mol. Cell Biol. *5*, 836–847.

Vassilopoulos, G., Wang, P.R., and Russell, D.W. (2003). Transplanted bone marrow regenerates liver by cell fusion. Nature *422*, 901–904.

Wang, X., Willenbring, H., Akkari, Y., Torimaru, Y., Foster, M., Al-Dhalimy, M., Lagasse, E., Finegold, M., Olson, S., and Grompe, M. (2003). Cell fusion is the principal source of bone-marrow-derived hepatocytes. Nature *422*, 897–901.

Weglarz, T.C., and Sandgren, E.P. (2000). Timing of hepatocyte entry into DNA synthesis after partial hepatectomy is cell autonomous. Proc. Natl. Acad. Sci. USA *97*, 12595–12600.

Weglarz, T.C., Degen, J.L., and Sandgren, E.P. (2000). Hepatocyte transplantation into diseased mouse liver. Kinetics of parenchymal repopulation and identification of the proliferative capacity of tetraploid and octaploid hepatocytes. Am. J. Pathol. *157*, 1963–1974.

Zhang, Y., Desai, A., Yang, S.Y., Bae, K.B., Antczak, M.I., Fink, S.P., Tiwari, S., Willis, J.E., Williams, N.S., Dawson, D.M., et al. (2015). Tissue regeneration. Inhibition of the prostaglandin-degrading enzyme 15-PGDH potentiates tissue regeneration. Science *348*, aaa2340.